Experimental Mechanics (2024) 64:839–849
https://doi.org/10.1007/s11340-024-01067-9

RESEARCH PAPER

A Dynamic Time Warping Approach to Access Fatigue Damage in Composite Pipes

M.V.L. Pazini[1] · L. de Abreu Corrêa[1] · H. Haan[1] · G. Zanon[2] · T.G.R. Clarke[1]

Received: 28 July 2023 / Accepted: 29 March 2024 / Published online: 17 April 2024

Abstract

Composite pressure vessels are seeing increasing demand in the oil and gas sector due to their excellent corrosion resistance. However, the assessment of the fatigue state of those structures still an open question. The goal of this work is use elastic wave data to access the fatigue damage (exudation). The Dynamic Time Warping method is proposed as a means of extracting features from guided wave ultrasound data that can describe the on-going fatigue induced damage of glass-fibre reinforced plastic pipes under fatigue-cycle loading. To test its efficiency, three pipe samples were fatigue tested to failure under internal pressure cycles with maximum values of 45 bar, 55 bar and 65 bar, and minimum pressures equal to 10% of the maximum, at a frequency of 0.8 Hz. A Guided Wave monitoring system consisting of a set of permanently attached piezoelectric sensors produced signals which were processed to obtain the Dynamic Time Warping distance, that was then used to obtain a Damage Index that expresses the cumulative fatigue damage suffered by the samples for each loading level. These results were comparable to data obtained from surface-mounted strain-gauges, even though temperature variations of up to 20 °C occurred during the tests and no direct temperature compensation was applied to the GW signals. The Dynamic Time Warping distance presents smaller influence of temperature and was able to better access the exudation of the samples.

Keywords SHM · Guided waves · Dynamic Time Warping · Composite pipes · Fatigue test · Damage assessment

Introduction

Composite pressure vessels are seeing increasing demand in the oil and gas sector due to their excellent corrosion resistance [1, 2]. Glass-Fibre Reinforced Plastic (GFRP) in particular is seen as a cheap substitute for carbon steels in a vast range of applications, such as in the chemical [3], water transportation [3, 4] and oil and gas industries [1, 5]. However, it is known that internal pressure cycling and long-term exposure to certain temperature ranges can lead to degradation of GFRP by fatigue [6–9] and creep mechanisms [10].

For fatigue loading, in particular, the two main damage mechanisms that arise in these materials are delamination and micro-cracks [11]. Micro-cracks develop at the matrix-fibre interface and act as stress concentration. As the number of cycles increases, micro-cracks grow and coalescence, leading to delamination [7, 11]. Fibre damage can also be present in the early stages of fatigue [12], but it is more relevant near the final failure of the component [13]. The presence of such defects eventually leads to permeation of the internal fluid, and at this stage, leaks and exudation can usually be observed on the surface of the vessel. In the context of composite pipes, exudation refers to the phenomenon in which the internal substance leaks or seeps from the composite material, often affecting the structural or functional integrity of the pipe. Visual inspections are usually incapable of detecting these defects before leakages have already occurred [14].

Fatigue damage in composites is often evenly distributed along the component [13], which causes a decrease in the stiffness of the material [8, 9, 15]. The stiffness behaviour of GFRP is often represented as a function of the number of fatigue cycles [12, 13, 16]. On Fig. 1, one can visualise the main characteristics of this curve. The fatigue process

✉ L. de Abreu Corrêa
labcorrea@gmail.com

[1] Post-Graduation Program in Mining, Metallurgy and Materials Engineering (PPGEM), Federal University of Rio Grande do Sul (UFRGS), 9500, Bento Gonçalves, Porto Alegre 90650-001, Rio Grando do Sul, Brazil

[2] Centro de Pesquisas e Desenvolvimento Leopoldo Américo Miguez de Mello (Cenpes), Petrobras, 950, Av. Horácio Macedo, Rio de Janeiro 21941-915, Rio de Janeiro, Brazil

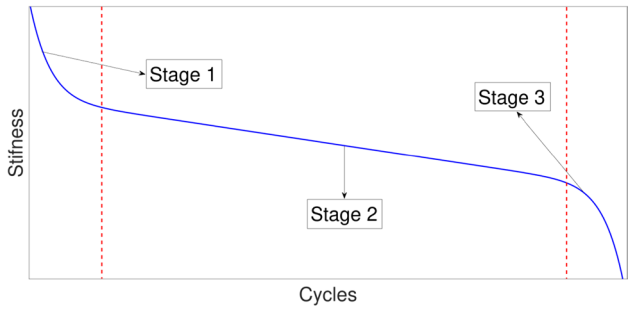

Fig. 1 Illustration of the stiffness qualitative behaviour of GFRP composites during fatigue

is divided into three stages: on the first stage, there is a significant drop in the stiffness with a relatively small number of cycles. This is followed by the second stage, which is characterised by a smaller and more constant rate of stiffness drop. Finally, on the third stage of the curve, there is a sharp drop of the stiffness culminating in the failure of the sample [12, 13, 16]. In some cases, however, the third stage may be absent [13].

Guided Waves

Compared with bulk ultrasonic waves, Guided Waves (GW) travels a longer distance in thin structures, which makes them suitable for application on highly attenuating materials [12], such as GFRP, some reviews about the subject can be found in [17–19]. Since the GW are capable to interact with large volumes of material [20, 21], they provide a more representative interrogation of the damage state of the structure. Furthermore, the sensors used to generate the GW can be lightweight, inexpensive, low profile and be permanently attached to the structure, allowing continuous monitoring, which are desirable characteristics for Structural Health Monitoring (SHM) applications [15, 22].

Since the GW velocity strongly depends upon the material's stiffness, a drop in the stiffness causes a drop in the GW velocity, which can be measured as an increase in the time-of-flight or a phase variation in the signal. Tao et al. [12] applied this principle to create a model to correlate the stiffness degradation with fatigue damage. Besides the effect in the signal's phase, the presence of fatigue defects also increases the attenuation of the material, resulting in a decrease in the wave's amplitude after propagation over a given distance [9]. Although both phase and amplitude are impacted by degradation in composite materials, and are viable metrics for detecting damage in GFRP pipes, it is imperative to underscore the incompatibility of their simultaneous use. Comparing amplitudes necessitates compensating for phase alterations, rendering it unfeasible to compute a metric that incorporates both simultaneously. Environmental factors can further complicate baseline measurements, predominantly influencing the phase shift of guided waves in composite pipes. Consequently, comparing amplitudes while compensating for phase shifts provides a more resilient metric against effects like temperature fluctuations [23, 24]. This will be explained in more detail, and examples of it will be given, in "Temperature Influence in the Distances" section.

Adden et al. [9], as well as, Mei and Giurgiutiu [25] employed acoustic attenuation measurements to evaluate the damage level of composites. Also, on the work created by Gao et al. [26], the authors used power spectrum density and cross-correlation methods to examine Lamb waves and coda waves. They used those methods to determine phase and amplitude variations to characterise debond defects present in honeycomb sandwich panels used in the aeronautical industry.

Furthermore, other approaches apply GW to evaluate the structural integrity of composites. For instance, Soleimanpour et al. [27] were capable of characterising delamination in laminated composite beams by the evaluation of acoustic non-linearity induced by those defects in A0 Lamb waves. Additionally, mode conversion can also be used to monitor the progression of fatigue damage. According to Zhang et al. [28], as the fatigue progresses, the mode conversion becomes more marked. Therefore, the authors successfully applied the mode-to-mode ratio measurements to assess the damage accumulated in GFRP. Similarly, Hosseini et al. [29] used mode conversion of guided waves for damage detection in cellular sandwich composites.

In this work, the Dynamic Time Warping (DTW) algorithm is proposed as a way of extracting information from GW signals regarding the occurrence of fatigue induced damage in glass-fibre composites. Thus, it was possible to monitor the effect on the stiffness of the material, the amplitude of the signals and the interaction between different GW modes simultaneously. The results were compared with strain-gauge measurements, corroborating the damage.

Distances Between Time Series

There are an several metrics to access the distance or dissimilarity between two distinct time series such as cross-correlation, Dynamic Time Warping and all the L_p norms. In this work we use the latter two methods as metrics to represent the fatigue damage induced in the composite pipe sample, where in our case the $p-norm$ is the L_2 (Euclidean distance).

Euclidean Distance - L_2 Norm

Comparisons between pairs of signals are performed to estimate the cumulative fatigue damage in GFRP pipes. To illustrate this, consider two generic time series representing GW signals obtained on a sample at different numbers of fatigue cycles Q and C, as described below:

$$Q = q_1, q_2, ...q_n$$

$$C = c_1, c_2, ...c_n$$

As mentioned, fatigue damage is expected to cause a variation in phase and amplitude between Q and C. There are several ways of calculating the variation between two time series; the most simple and often used method is the Euclidean distance which is defined, by equation (1) as:

$$L_2(Q, C) = \sqrt{\sum_{n=1}^{n}(q_i - c_i)^2} \tag{1}$$

Equation (1) shows that the L_2 is simply the square root of the sum of the square of the differences in the amplitudes between points of the two time series. In this case, there is no regard for evident phase shifts that might be present, as a result, the distances between points are linear and point-to-point (as seen in Fig. 2(a). This means that, if the signals are misaligned or out of phase, the computed Euclidean distance will be unreasonably large [30].

Dynamic Time Warping Algorithm

Dynamic time warping (DTW) is a technique commonly used to find an optimal alignment between two time series. This method warps two time series in a non-linearly fashion to match each other [31, 32]. This means that DTW is capable of correcting synchronisation errors between two time series [32].

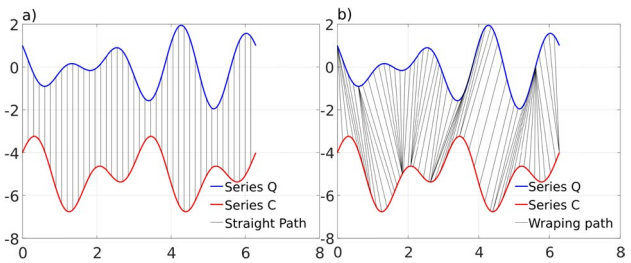

Fig. 2 (**a**) L_2 distance between two time series with linear alignment, the one-to-one linear mapping between the series is represented by the black vertical lines. (**b**) DTW alignment between two time series, the black lines connecting the series Q and C are the optimal matching points found by the DTW algorithm

Figure 2(b) presents an example of the alignment between two similar out of phase time-dependent sequences. In this case, it can be observed that not all points are related vertically, but some are related in a shifted fashion. This is due to the optimal match found by the algorithm.

DTW was initially used to compare different speech patterns in automatic speech recognition [31, 33]; however, it is also possible to use this algorithm to compute DTW distance for the classification of other time-dependent sequences as well [33–36]. For example, the DTW algorithm can be used to optimally align and calculate the distance of two GW time-series as in the case of Q and C, which may be out of phase or with different velocities (i.e. due to temperature changes) [34, 35].

The DTW algorithm begins by creating a matrix M, often called cost matrix, with size n-by-m where each element of this matrix consists of the distance between the points q_i and c_j (equation (2)). One way to construct the cost matrix is by the computation of the distance of each element in the Cartesian product between the series [31] Q and C, as seen in equation (3).The definition of distance used in equation (2) depends on the type of information one aims to obtain. The Euclidean distance captures the difference between the time series, whereas distances based on entropy metrics (e.g., Kullback–Leibler Divergence) represent the difference between the probability distributions of these time series.

$$d_{i,j} = ||q_i - c_j|| \tag{2}$$

$$M = d(Q \times C) = \begin{bmatrix} d(q_1, c_N) & \cdots & d(q_N, c_M) \\ \vdots & \ddots & \vdots \\ d(q_1, c_1) & \cdots & d(q_N, c_1) \end{bmatrix} \tag{3}$$

A warping path w is created by choosing some elements of M as it defines the mapping between Q and C. As each w_k is an element of M and each element in M is a distance between a point in Q and a point in C, w is a vector on which each position is a distance between the sequence Q and C.

The best match between series Q and C is found by choosing the elements of M that minimise the total cumulative distances between the series (equation (4)) and the choice of those elements are subjected to the following constraints [37]:

- The initial and final points must be the first and last points in the alignment, $w_1 = M_{1,1}$ and $w_k = M_{m,n}$
- Monotonicity of the path, which means the path does not decrease: $w_i \leq w_{i+1}$
- The DTW path must be continuous and advance one step at a time.

$$DTW(Q, C) = argmin\left\{ \sum_{k=1}^{K} \sqrt{w_k} \right\} \tag{4}$$

Usually, the optimal path in the matrix M is found with a dynamic programming technique [30, 31, 37]. In dynamic programming, the solution of DTW is found by evaluating the recurrence expression presented in equation (5). This equation defines the cumulative distance $D(i, j)$ in the current position as the minimum cumulative distances in the adjacent elements. An example of the optimal warping path found by DTW can be seen in Fig. 3. There, the cost matrix M calculated for the sequences C and Q is shown as a colour map and the red line represents the warping path found by the algorithm. The warping path also follows all the constraints since the initial and final points match the first and last points of the alignment, the line is continuous and monotonic.

$$D(i,j) = d(q_i, c_j) + ... \\ min(D(i-1,j), D(i,j-1), D(i-1,j-1)) \quad (5)$$

Experimental Procedure

Experimental Setup and Composite Samples

The GFRP pipes used in the tests were manufactured using two polyester veils (25 g/m^2) and two E-CR glass-fibre veils (300 g/m^2) to create a chemical barrier on the inner surface of the pipes. On top of the chemical barrier, it was used the filament winding technique to deposit 12 layers of E-CR fibres (1100 g/km) oriented at ±55°, which were responsible for the structural strength. Both the chemical barrier and structural glass-fibre were joined with bisphenol A epoxy resin, resulting in a 150 mm internal diameter pipe with a thickness of 4.40 mm ($D/t = 34$).

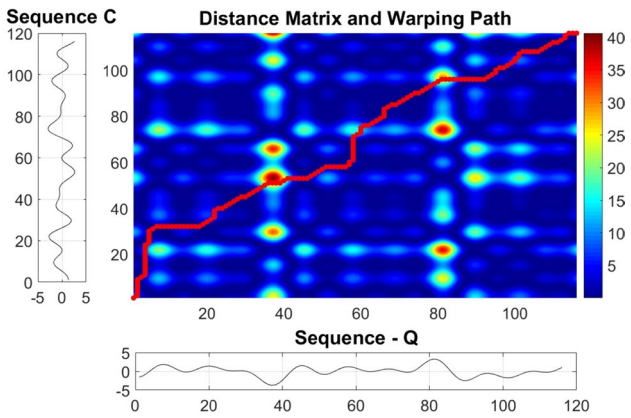

Fig. 3 Colour map of the cost matrix M between sequences C and Q. The warping path W between the two time series represented in red, the path is monotonic, continuous with beginning and ending in the first and last points of each series

These pipes were instrumented with a strain-gauge to monitor the deformations in the circumferential direction and observe how the elastic modulus changes during the fatigue test. The technique of resistance strain gauging was employed to measure deformations during the fatigue test. Deformation monitoring was conducted using three pairs of sensors—one longitudinally and the other circumferentially positioned. The central region of the tube was chosen for instrumentation, with each sensor pair phased at 120°. Given the prolonged nature of the test, acquisitions were performed in 10-second blocks with a 10-minute interval between each block, at a sampling frequency of 100 Hz. Uni-axial strain gauges with an active sensor length of 5 mm from the manufacturer Micro-Measurements-VPG were utilized to measure deformations during the fatigue test. The QuantumX universal data acquisition system from HBM, Hottinger Baldwin Messtechnik, was used for data acquisition. The Catman version 5.4.2 software, provided by the equipment manufacturer, was employed for data acquisition.

Furthermore, a pair of ultrasonic piezoelectric sensors were installed 157 mm (equivalent to 120°) apart of each other to be used to generate and detect GW in the circumferential direction. The circumferential path was chosen because, in a field scenario where the pipeline may be buried or have other access restrictions, this makes guided wave instrumentation simpler, as only a relatively small section needs to be exposed for instrumentation. Additionally, it was expected that, due to the internal pressure cycling of the pipe, damage mechanisms would nucleate and expand as a consequence of the induced hoop stress, and circumferential waves would thus be interrogating the pipe in the most critical direction, possibly leading to a greater response. For guided wave signal generation, the signal generator model 33521 - LXI from Agilent Technologies was used, producing a wave with a generation frequency of 20 MHz connected to the broadband signal amplifier model 7602 M from Krohn-Hite Corporation. A preamplifier from McWade Monitoring Ltd was employed for sensor reception, with the gain set at 40 dB. Finally, the oscilloscope model DSOX3034A from Agilent Technologies was used for signal acquisition at a sampling frequency of 2 MHz.

The fully instrumented GFRP pipe, as well as a schematic with the dimensions of the pipe and positioning of the sensors is shown in Fig. 4. The sensors had a 6.35 mm-diameter, 0.25 mm-thickness and were vertically polarised, for more information refer to a single sensor from Acellent (https://www.acellent.com). These sensors were excited with a 5-cycle Hanning-windowed tone-burst at a centre frequency of 150 kHz. At these frequencies, the sensors generate mostly out-of-plane displacement, which means that the main modes expected to be generated are anti-symmetric. No major effort was made to characterise the GW modes generated in the test pieces in this paper; also,

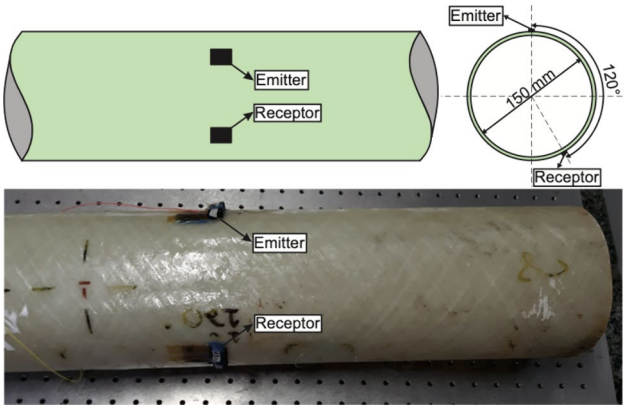

Fig. 4 Instrumented pipe with piezoelectric sensors, the schematic shows the emitter and receptor placement 120° apart of each other

no attempt to filter out undesirable modes was performed. From the perspective of homogenisation, the greater the ratio between the distance travelled by the wave and the wavelength, the more information about the medium through which the wave propagates is captured [38, 39]. However, as the frequency increases, the attenuation suffered by the guided wave also increases, causing the signal captured by the sensor to become very low, lower than the electromagnetic noise picked up by the instrumentation. This makes the use of higher frequencies impractical. It is necessary to find a compromise between propagation distance and wavelength. Finally, it is not strictly necessary to fully characterise the wave modes propagated by the sensor in this structure. Anti-symmetric modes have higher excitability [40] than other modes, are it also has been shown that they are adequate for detection of delamination in composites [41], but since the proposed methods are data-driven, the presence of other modes can be beneficial as they provide additional sources of statistical information for the methods.

As a result, the entire time series was used in the data analysis. This resulted in all the modes contributing to the signal being taken into account by the DTW algorithm. To obtain the time series used in this work, the GW signal was averaged over 512 data acquisitions to reduce the influence of electromagnetic white noise. The data was recorded at 0 bar pressure. Later, the data was processed to obtain the normalised Damage Index (DI) feature. The three samples were tested in similar ambient conditions, in which uncontrolled temperature variations of up to 10.6 °C were recorded. It is known that temperature variation can influence GW measurements [15]; however, no specific temperature compensation techniques (such as [23, 24] were applied in the signal processing procedures.

Three pipes were cyclically pressurised to induce fatigue damage up to failure, which was considered when exudation started to appear on the surface of the pipe. The loading frequency was 0.8 Hz in all cases with a load ratio (R) equal to 0.1. The fatigue test frequency was chosen as the maximum frequency the hydraulic equipment was capable of operating at. The equipment used for applying mechanical loading during the fatigue test was an actuator, Servohydraulic Test System model from MTS System Corporation. The software used for configuration and control of the actuator was MTS TestSuite version 4.0 provided by the equipment manufacturer. For pressure data acquisition, the QuantumX universal data acquisition system from HBM was employed. In conjunction with the acquisition system, the pressure transducer with a nominal capacity of up to 500 bar, model P8AP, also from HBM was used as the pressure transducer during the fatigue test. The software used for QuantumX control was Catman version 5.4.2 provided by the equipment manufacturer. The acquisition frequency was 100 Hz. The rupture pressure of the pipes (P_r) was determined to be equal to 180 bar via a quasi-static pressurisation test carried out on a fourth sample.

Table 1 Experimental parameters

Sample	Pmin [bar]	Pmax [bar]	Pmax/Pr
1	4.5	45	0.250
2	5.5	55	0.306
3	6.5	65	0.361

To complete the fatigue tests in a reasonable time, the maximum applied pressure (P_{max}) was chosen to result in a number of cycles to failure ranging from 10^4 Pa to 10^5 Pa order of magnitude. Table 1 shows the minimum applied pressure (P_{min}), P_{max} and the ratio between P_{max} and P_r. Figure 5, shows a schematic of the equipment utilised for control and application of pressure in the pipes. The control station is responsible for keeping track of the number of cycles and for controlling the hydraulic pump. The hydraulic scheme shows that the pump pressurises the oil from the reservoir into the hydraulic cylinder, which causes the actuator to move back and forward. This results in pressurisation cycles in the water-filled pipe and damage by fatigue on the sample.

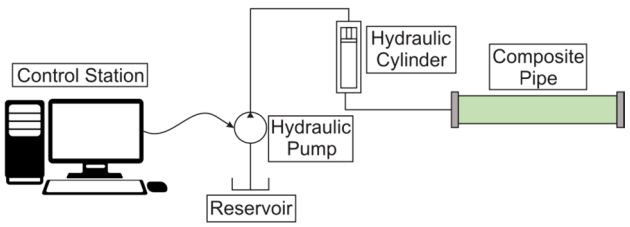

Fig. 5 Schematic of the experimental setup, the control station is responsible for controlling the hydraulic pump, which moves the actuator of the hydraulic cylinder, increasing and releasing the pressure to create pressure cycles inside the GFRP pipe

As reference technique for the damage degradation we use strain-gauge and pressure measurements. Assuming the plane stress hypothesis, the pressure can be convert to stress as follow:

$$\sigma_{zz} = \frac{pR_0}{t_0}, \quad \sigma_{rr} = 0, \quad \sigma_{\theta\theta} = \frac{P}{2\pi R_0 t_0} + \frac{pR_0}{2t_0}, \tag{6}$$

where p is the internal pressure, $P = \pi p R_0^2$, R_0 is the mean radius and t_0 in the thickness. Now we are able to evaluate the relation between stress and strain. Now,the stress and strain can be used to evaluate the Young's Modulus.

Temperature Influence

In our experiment we do not control the temperature, anyhow we monitored its value. During operation is almost impossible to accurately control the pipe's temperature, due to environmental and installation issues. However, the change in temperature can lead to alteration in signals that, if not taken into consideration, could lead to miss interpretation of experimental results and possibly create false results regarding the pipe's structural integrity.

To address this issue, we performed one experiment in a pristine GFRP pipe from the same batch, without any kind of mechanical load. We kept all the GW setup as presented above. Type K thermocouples from HBM were used for temperature control. These were positioned 10 mm away from the piezoelectric sensors on the external surface of the tube. To facilitate heat transfer between the tube wall and the thermocouple, thermal paste was used. In order to minimise the effects of external temperature, a fibreglass blanket approximately 60 mm thick was used as insulation around the thermocouple. This enabled obtaining a temperature measurement very close to the temperature of the piezoelectric sensor attached to the external surface of the tube. For temperature data acquisition, the QuantumX universal data acquisition system from HBM was used. The software used for data acquisition was Catman version 5.4.2 with a sampling frequency of 100 Hz. For heating, a heater made in the laboratory was used. It was connected to the temperature controller N1040 from the company NOVUS, using thermocouple 1 as a reference.

Figure 6 shows the temperature profile obtained in the test. Where the x marker is the thermocouple 1, the dot marker is the thermocouple 1, and the square marker is the thermocouple 3. The dashed line is the mean value of the temperature. The mean value was assumed as the value of the GFRP pipe sample. One guided wave measurement was made at each temperature resulting in 18 GW tests in total.

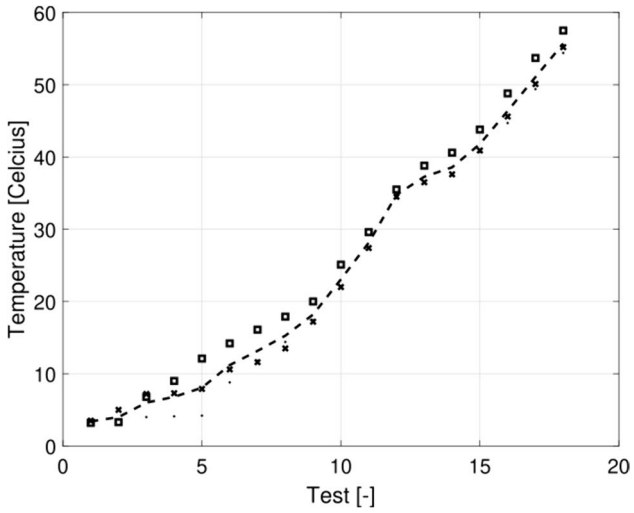

Fig. 6 Temperature profile obtained in the test. Where the 'x' marker is the thermocouple 1, the marker 'dot' is the thermocouple 1, and the 'square' marker is the thermocouple 3. The dashed line is the mean value of the temperature

Results and Discussion

Temperature Influence in the Distances

Figure 7 shows the influence of the temperature in the recorded raw data. The blue line is one guided wave signal recorded at 3.4 °C. The cyan line is one guided wave signal recorded at 18.0 °C. The magenta line is one guided wave signal recorded at 55.7 °C. In the inset plot we can see two regions in detail, both present similar behaviour, a phase shift to the right. It is due to some reduction in the energy velocity. Another clear feature present is the reduction of the amplitude with the temperature. However, for the region around 0.3 ms we note a very small amplitude for the lowest temperature, on another hand, at 18.0 °C we note higher amplitude. This change of behaviour shows the complex phenomena present in the guided wave results. It can lead to a wrong interpretation of the DI.

Figure 8 shows the temperature influence in the norm L_2 (right y-axis) and DTW (y-left axis). They present a very similar behaviour with a high slope around 10 °C and a smooth decrease up to around 40 °C when higher negative slope. All all recorded GW data are within the range of 10 °C to 40 °C (the vast majority of them between 20 °C and 30 °C). This small variation of the metric allows us to affirm that variations in the metric higher than the variations presented below are not provident from the temperature variation during the records.

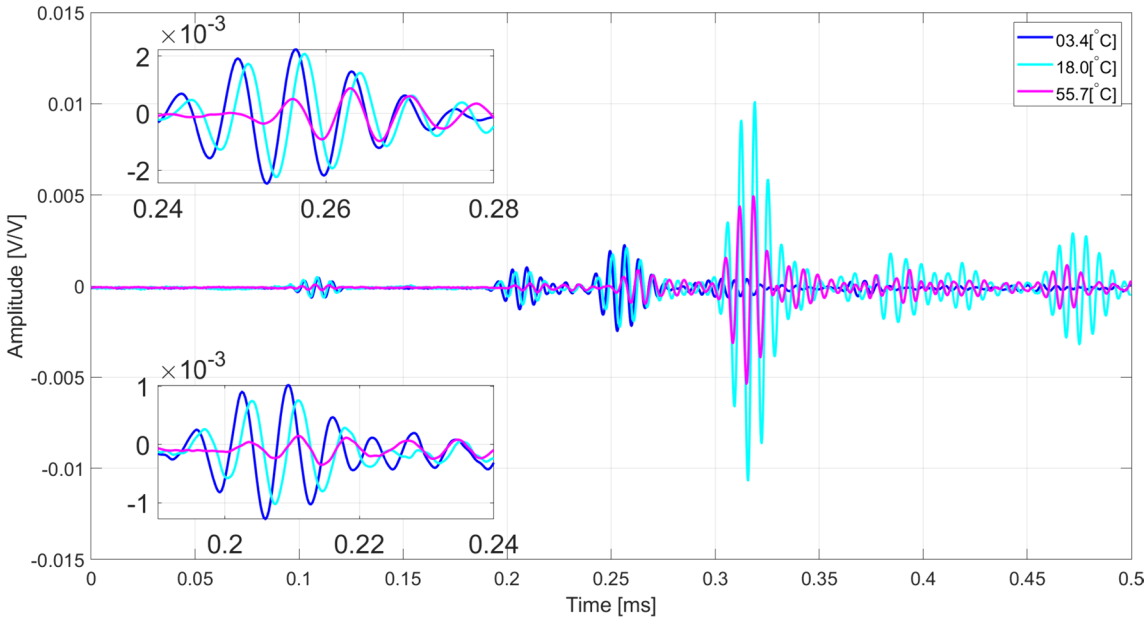

Fig. 7 Influence of the temperature in the recorded raw data. The blue line is one guided wave signal recorded at 3.4 °C. The cyan line is one guided wave signal recorded at 18.0 °C. The magenta line is one guided wave signal recorded at 55.7 °C

Composite Degradation Patterns

As an example of the behaviour of the raw data throughout the fatigue test, Fig. 9 shows the first GW envelope to arrive at the transducer for the 55 bar sample at 0, 7000 and 22500 cycles. In this figure, it is possible to notice that the amplitude of the signal drops with the increase of the number of cycles. This behaviour was observed in all the data sets and it is due to the progressive increase of the acoustic attenuation during the fatigue test. On the other hand, Fig. 9 also shows that the signal shifts back and forth, mainly due to the temperature variations, which makes it difficult to predict its response. Because of the phase variations, direct comparison of the data through simple Euclidean or through conventional time-dilation methods are difficult or impracticable.

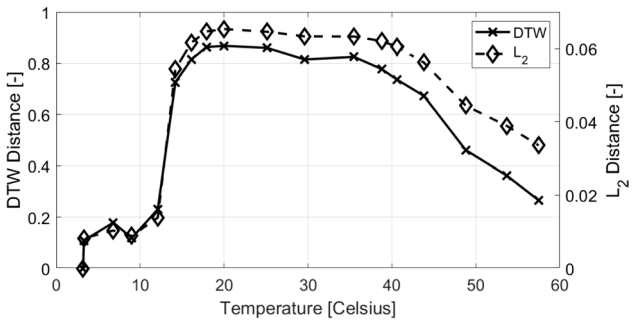

Fig. 8 DI distance variation Vs Temperature

Results from the strain-gauge method are displayed in Fig. 10 as a reference for the L_2 and DTW results to be presented in the next sections. The strain-gauge results are displayed as the variation of the elastic modulus in the circumferential direction as a function of the normalised number of cycles for the three tested samples.

Time Series Evaluation with L_2 and DTW

For the time series evaluation of GW signals, one signal sample from each pipe was collected before the beginning of the fatigue

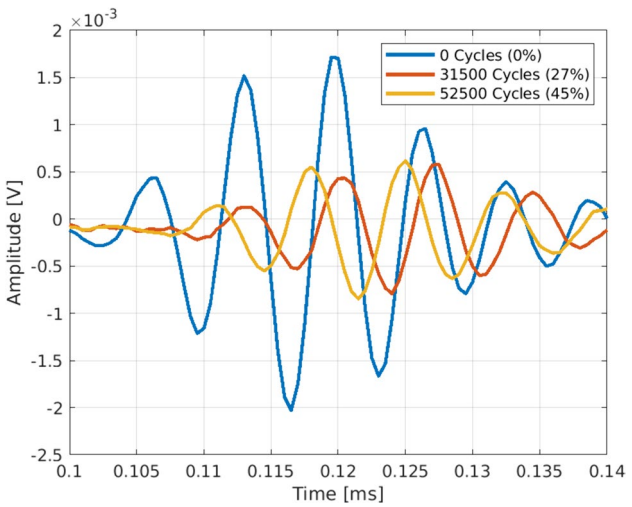

Fig. 9 Ultrasound signals from the sample 2 at different number of cycles. As the number of cycles increases, the amplitude of the waves decreases and the phase moves back and forward

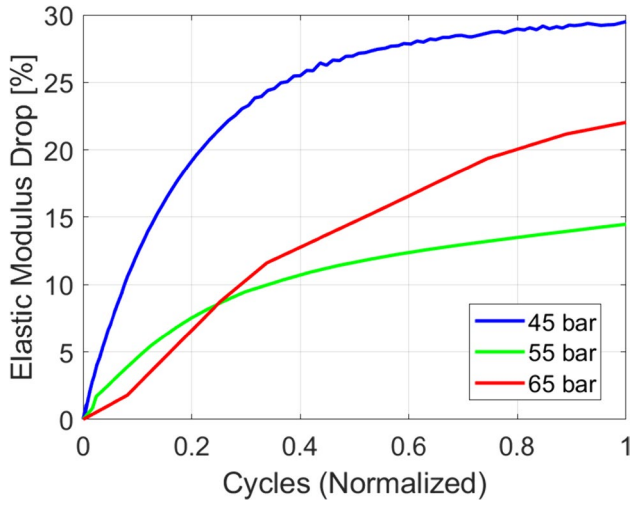

Fig. 10 Drop of the elastic modulus measured with strain-gauge as a function of the number of cycles for the three samples analysed (%)

process, this signal is called baseline. Then the baseline is compared with every signal collected afterwards, this comparison is done by means of calculating the L_2-norm and the DTW.

The DTW algorithm applied to the GW signals resulted in two outputs, the mapping of the baseline and the fatigue signals as well as the DTW distance between them. Figure 11 shows the results of applying both methods to access the distance of GW time series.

Observing Fig. 11 one can notice the irregularity of the L_2 especially in the case of the 45 bar fatigue process (Fig. 11(a)) when compared with the DTW method (Fig. 11(b)), this behaviour is undesired for establishing a good measure of lifespan in composite pipes and is likely originated for the lack of compensation for phase changes. Thus the distances obtained through the application of the DTW method are a more stable and reliable way of measuring distances between signals of pipes that endured some sort of fatigue process.

Figure 11(a) and (b) show higher DI amplitudes for the 45 bar tests. This result is in accordance with the observations

Fig. 11 Comparison between the norm distances of fatigue cycles in different pressures

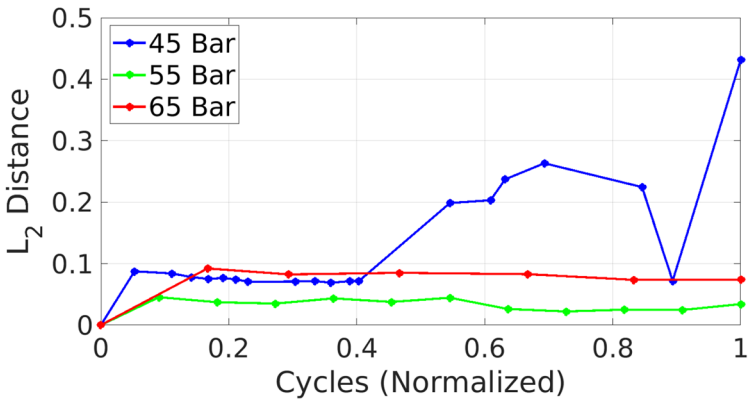

(a) Distances from baseline signal calculated with L_2-norm.

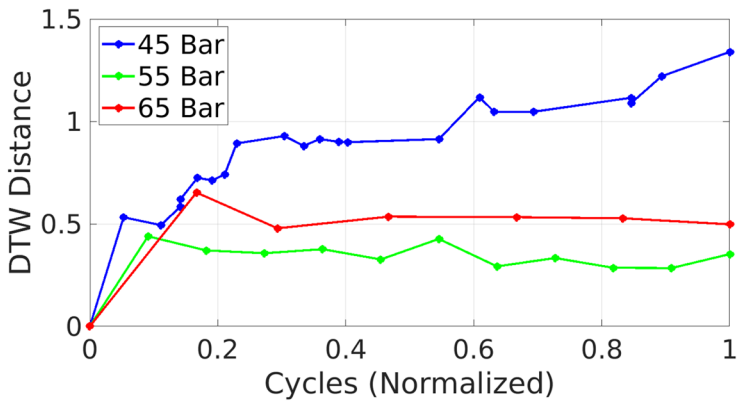

(b) Distances from baseline signal calculated with DTW metric.

made during the tests. The micro-cracking damage [42] of matrix produces a colour variation in the composite. During testing, it was observed that for instances where the pressure differential (ΔP) was minimal, the damage manifested uniformly across the specimen. Conversely, at 55 bar and 65 bar, where ΔP was higher, the colour variations intensified but were localised in multiple areas, distributed along both the length and circumference of the pipe sample. Consequently, some damaged regions were situated beyond the path of emitter-receptor pairs, thus not contributing to the incremental rise in DI as observed in the 45 bar test, which resulted in a lesser DI measurement for these samples.

The one similarity between both methods is that given the range of temperatures measured during the experimental procedure is between 20 °C and 40 °C, both of them present very low variation regrading the calculated distance and temperature changes, thus implying that temperature effects cannot mask fatigue induced damages. Figure 8 shows that for the DTW method the difference between distances at 20 °C and 40 °C is as low as 0.08 and for the L_2 metric is 5×10^{-3} representing respectively 22.7% and 175% of the lowest distance ever measured for a pipe that met the failure criteria in this work.

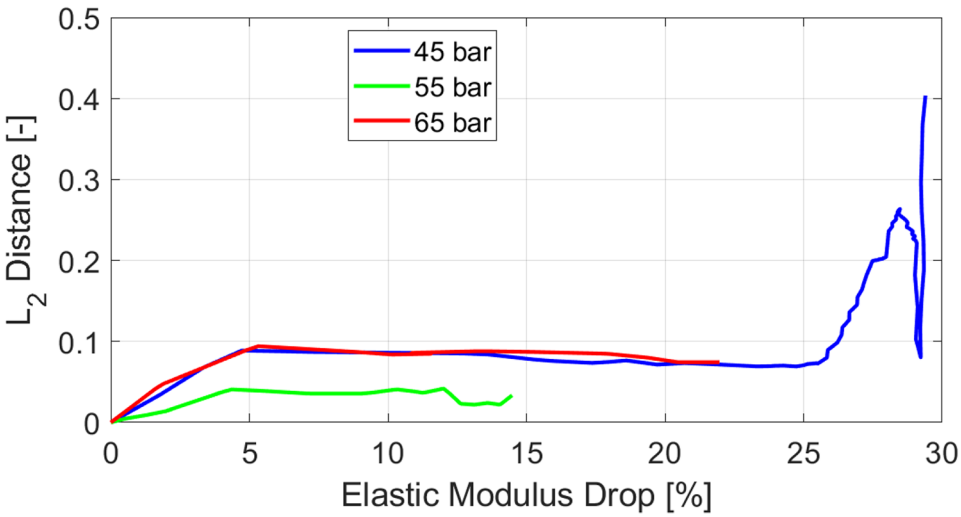

(a) Elastic modulus drop vs L2 damage.

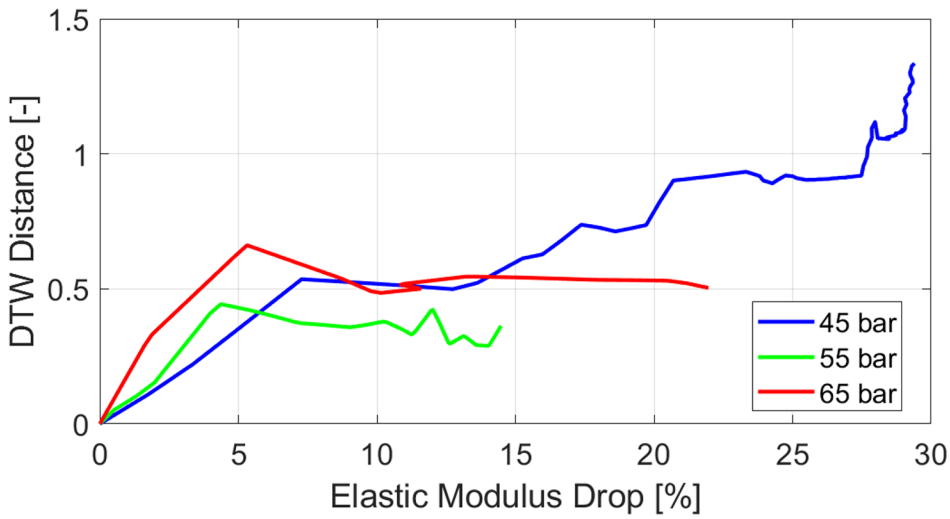

(b) Elastic modulus drop vs DTW damage.

Fig. 12 Elastic modulus drop vs norm distances

Correlation between Elastic Modulus Drop and Distance Metrics

"Composite Degradation Patterns" section shows the elastic modulus drop measured by the strain gauges (Fig. 10). The DTW distance and the Euclidean distance were obtained in "Time Series Evaluation with L_2 and DTW" section (Fig. 11(a) and (b)). The next step is to check the relation between those quantities.

As shown in Fig. 10, one can see that the sensitivity of the decay reduces dramatically, this is also a classical result, as presented in the literature, corresponding to state 2 in Fig. 1. This creates a problem for the sensitivity of any composite damage detection method.

In Fig. 12(a), is possible to observe that the L_2 was not constant in correlating the elastic modulus drop with the distances between the signals during the fatigue tests, this might be the case due to the lack of phase shift compensation inherent of the L_2 Distance measurement. This can be seen in Fig. 12(a), where a plateau is installed at 5% loss of modulus of elasticity.

Figure 12(b) shows a more constant relation between the degradation measured by sensors and the distance of time series, thus indicating that the DTW method is a better option, when compared to L_2, to access the damage caused by fatigue with GW data.

To summarise, both metrics can obtain a linear relationship in the first stages, but only DTW at low fatigue pressure captures stage 2 pressure vessel degradation. For the DTW standard, at 45 bar, a behaviour with approximately two regimes is observed, one up to 5% and the other from there on (the inclination of the line changes). Unfortunately, for higher pressures, as the damage is not extended throughout the sample, but located in more concentrated regions, the DTW and L_2 distance fails.

Conclusion

This paper presents a comparison between L_2 and DTW distance of GW signals obtained from glass-fibre reinforced polymer pipes subjected to fatigue. We concluded the following:

- Temperature Influence: The study explored the impact of temperature on guided wave signals. Variations in temperature caused phase shifts and reduction in amplitude, leading to a complex interpretation of the DI and the potential for misinterpretations. However, the variations in DTW distance due to temperature changes were relatively small.
- Composite Degradation Patterns: The behaviour of raw data throughout fatigue tests was investigated. As the number of fatigue cycles increased, there was a noticeable drop in the amplitude of guided wave signals due to the progressive increase in acoustic attenuation during the fatigue test. Additionally, the signals exhibited phase shifts caused by temperature variations, making direct comparisons challenging using conventional methods.
- Distance Metrics: The evaluation of time series with two distance metrics, L_2 and DTW, was compared. DTW showed more stable and reliable measurements of distances between signals subjected to fatigue processes compared to the irregularities observed in the L_2 distances. This indicated that DTW was a better option for assessing fatigue-induced damage using guided wave data.
- Correlation with Elastic Modulus Drop: The study examined the correlation between the elastic modulus drop measured by strain gauges and the distance metrics. DTW displayed a more consistent relationship between degradation measured by sensors and the distance of time series, making it a preferable option for assessing fatigue-induced damage. However, at higher pressures, where damage was concentrated in specific regions, both DTW and L_2 distance metrics showed limitations.

Acknowledgements The authors would like to thank the Petrobras for sponsoring this research, especially Cláudio Jarreta for his support. The authors are also thankful for the help received throughout this research from the following LAMEF members: Toni R. S. de Lima, Felipe Lutckmeier, Daniel S. da Silva, Juliano W. Silva, Rodrigo M. Praetzel and Lucas A. Schmidt. Prof. Dr. Thomas G.R. Clarke would like to acknowledge funding provided through the CAPES-PROEX Program of PPGE3M and through the productivity scholarship provided by CNPq.

Data Availability The data that support the findings of this study are available from the corresponding author upon reasonable request.

Declarations

Conflict of Interest The authors declare that they have no conflict of interest.

References

1. Hastie JC, Kashtalyan M, Guz IA (2019) Failure analysis of thermoplastic composite pipe (TCP) under combined pressure, tension and thermal gradient for an offshore riser application. Int J Press Vessels Pip 178:103998
2. Rohem N, Pacheco L, Budhe S, Banea M, Sampaio E, De Barros S (2016) Development and qualification of a new polymeric matrix laminated composite for pipe repair. Compos Struct 152:737–745
3. Sebaey TA (2019) Design of oil and gas composite pipes for energy production. Energy Procedia 162:146–155
4. Chakraverty A, Dash S, Maharana H, Beura S, Mohanty U (2020) A novel investigation on durability of GRE composite pipe for prolonged sea water transportation. Compos Commun 17:42–50

5. Ferreira C, Lopes R, Santos T, Oliveira D, Martins F, Pereira G (2020) Non-destructive inspection of laminated pipe joints in polymeric composite material reinforced by fiberglass. Nucl Instrum Methods Phys Res Sect A 954:161154
6. Rafiee R (2017) Stochastic fatigue analysis of glass fiber reinforced polymer pipes. Compos Struct 167:96–102
7. Beaumont P, Dimant R, Shercliff H (2006) Failure processes in composite materials: getting physical. J Mater Sci 41(20):6526–6546
8. Yadav IN, Thapa KB (2020) Fatigue damage model of woven glass-epoxy fabric composite materials. J Market Res 9(1):301–306
9. Adden S, Pfleiderer K, Solodov I, Horst P, Busse G (2008) Characterization of stiffness degradation caused by fatigue damage in textile composites using circumferential plate acoustic waves. Compos Sci Technol 68(7–8):1616–1623
10. Lavergne F, Sab K, Sanahuja J, Bornert M, Toulemonde C (2015) Estimation of creep strain and creep failure of a glass reinforced plastic by semi-analytical methods and 3D numerical simulations. Mech Mater 89:130–150
11. Harris B (2003) Fatigue in composites: science and technology of the fatigue response of fibre-reinforced plastics. Woodhead Publishing
12. Tao C, Ji H, Qiu J, Zhang C, Wang Z, Yao W (2017) Characterization of fatigue damages in composite laminates using lamb wave velocity and prediction of residual life. Compos Struct 166:219–228
13. Movahedi-Rad AV, Keller T, Vassilopoulos AP (2018) Fatigue damage in angle-ply GFRP laminates under tension-tension fatigue. Int J Fatigue 109:60–69
14. Larrosa C, Lonkar K, Chang F-K (2014) *In situ* damage classification for composite laminates using gaussian discriminant analysis. Struct Health Monit 13(2):190–204
15. Saeedifar M, Mansvelder J, Mohammadi R, Zarouchas D (2019) Using passive and active acoustic methods for impact damage assessment of composite structures. Compos Struct 226:111252
16. Peng T, Liu Y, Saxena A, Goebel K (2015) *In-situ* fatigue life prognosis for composite laminates based on stiffness degradation. Compos Struct 132:155–165
17. Su Z, Ye L, Lu Y (2006) Guided lamb waves for identification of damage in composite structures: a review. J Sound Vib 295(3–5):753–780
18. Gholizadeh S (2016) A review of non-destructive testing methods of composite materials. Procedia Structural Integrity 1:50–57
19. Mitra M, Gopalakrishnan S (2016) Guided wave based structural health monitoring: a review. Smart Mater Struct 25(5):053001
20. Ricci F, Monaco E, Maio L, Boffa ND, Mal AK (2016) Guided waves in a stiffened composite laminate with a delamination. Struct Health Monit 15(3):351–358
21. Altabey WA, Noori M (2017) An extensive overview of lamb wave technique for detecting fatigue damage in composite structures. Industrial and Systems Engineering, American Institute of Science 2(1):1–20
22. Giurgiutiu V (2015) Structural health monitoring of aerospace composites. Academic Press
23. Clarke T, Simonetti F, Cawley P (2010) Guided wave health monitoring of complex structures by sparse array systems: Influence of temperature changes on performance. J Sound Vib 329(12):2306–2322
24. Mariani S, Heinlein S, Cawley P (2020) Compensation for temperature-dependent phase and velocity of guided wave signals in baseline subtraction for structural health monitoring. Struct Health Monit 19(1):26–47
25. Mei H, Giurgiutiu V (2019) Guided wave excitation and propagation in damped composite plates. Struct Health Monit 18(3):690–714
26. Gao F, Wang L, Hua J, Lin J, Mal A (2021) Application of lamb wave and its coda waves to disbond detection in an aeronautical honeycomb composite sandwich. Mech Syst Signal Process 146:107063
27. Soleimanpour R, Ng C-T, Wang CH (2017) Higher harmonic generation of guided waves at delaminations in laminated composite beams. Struct Health Monit 16(4):400–417
28. Zhang C, Zhang Z, Ji H, Qiu J, Tao C (2020) Mode conversion behavior of guided wave in glass fiber reinforced polymer with fatigue damage accumulation. Compos Sci Technol 192:108073
29. Hosseini S, Duczek S, Gabbert U (2014) Damage localization in plates using mode conversion characteristics of ultrasonic guided waves. J Nondestr Eval 33(1):152–165
30. Ratanamahatana CA, Keogh E (2004) Making time-series classification more accurate using learned constraints. Proceedings of the 2004 SIAM International Conference on Data Mining. SIAM, pp 11–22
31. Müller M (2007) Information retrieval for music and motion, vol 2. Springer
32. Dexter E, Pérez P, Laptev I (2009) Multi-view synchronization of human actions and dynamic scenes. British Machine Vision Conference Proceedings. pp 1–11
33. Jeong Y-S, Jeong MK, Omitaomu OA (2011) Weighted dynamic time warping for time series classification. Pattern Recogn 44(9):2231–2240
34. Douglass A, Harley JB (2017) Dynamic time warping for temperature compensation in structural health monitoring. AIP Conference Proceedings, vol 1806. AIP Publishing LLC, p 020017
35. Galarza N, Rubio B, Diez A, Boto F, Gil D, Rubio J, Moreno E et al (2016) Implementation of Signal Processing Methods in a Structural Health Monitoring (SHM) System based on Ultrasonic Guided Waves for Defect Detection in Different Materials and Structures. In Proceedings of the 8th European Workshop On Structural Health Monitoring (EWSHM 2016)
36. Kim S, Kim NH, Choi J-H (2020) Prediction of remaining useful life by data augmentation technique based on dynamic time warping. Mech Syst Signal Process 136:106486
37. Sakoe H, Chiba S (1978) Dynamic programming algorithm optimization for spoken word recognition. IEEE Trans Acoust Speech Signal Process 26(1):43–49
38. Auriault J-L, Boutin C, Geindreau C (2010) Homogenization of coupled phenomena in heterogenous media. John Wiley & Sons, p 149
39. Cottereau R (2016) Scale coupling and upscaling techniques in elastostatics and elastodynamics in random media. PhD thesis, Université Pierre & Marie Curie-Paris 6
40. Wilcox PD, Lowe MJS, Cawley P (2005) The excitation and detection of lamb waves with planar coil electromagnetic acoustic transducers. IEEE Trans Ultrason Ferroelectr Freq Control 52(12):2370–2383. https://doi.org/10.1109/TUFFC.2005.1563281
41. Ramadas C, Balasubramaniam K, Joshi M, Krishnamurthy CV (2011) Numerical and experimental studies on propagation of a0 mode in a composite plate containing semi-infinite delamination: observation of turning modes. Compos Struct 93(7):1929–1938. https://doi.org/10.1016/j.compstruct.2011.01.025
42. Talreja R (1981) Fatigue of composite materials: damage mechanisms and fatigue-life diagrams. Proceedings of the Royal Society of London. A. Mathematical and Physical Sciences 378(1775):461–475